A THREE-DIMENSIONAL NUMERICAL ANALYSIS OF COMPLETE CROSSFLOW HEAT EXCHANGERS WITH CONJUGATE HEAT TRANSFER

M. Perčić[1*] – K. Lenić[1] – A. Trp[1]

[1]Dept. of Thermodynamics and Energy Engineering, Faculty of Engineering, University of Rijeka, Vukovarska 58

ARTICLE INFO

***Article history*:**
Received 18.07.2012.
Received in revised form 07.12.2012.
Accepted 07.12.2012.

Keywords:
Fin-and-tube heat exchanger
Crossflow heat exchanger
Numerical analysis
Heat transfer
Conjugate heat transfer
Air-side and water-side
Non-constant physical properties

Abstract:

In this paper, a three dimensional numerical analysis of turbulent fluid flow and heat transfer on the air-side and water-side of plain fin-and-tube heat exchangers is performed in order to obtain their heat transfer characteristics with non-constant physical properties. Besides convection heat transfer on water and air sides, the heat conduction through pipe walls and fins is also considered in the study. The two types of heat exchangers having cascade and in-line flat tube arrangements are presented.. Heat exchangers have been numerically simulated for different inlet air temperatures and velocities. As crossflow has been taken into account, the heat exchangers have been modeled with all fins considering the temperature changes on both sides. Numerical values are compared to the results obtained by analytical calculations of the heat exchangers, and good agreement of results is derived. The heat transfer characteristics are observed to be better for the heat exchanger with cascade tube arrangement for all of the analyzed conditions.

1 Introduction

An efficient use of energy in its primary form of heat is of paramount importance for energy efficiency in general. One of the basic common components of numerous thermal devices and thermal systems are the heat exchangers. It is logical to assume that the goal of energy efficiency of thermal facilities is achievable only by increasing the efficiency of its components i.e. heat exchangers. Heat exchangers are devices which are used for transferring heat energy efficient between two or more fluids divided by a solid wall or when being in contact. The thermal efficiency of a heat exchanger depends on various operating and geometry characteristics, and therefore, an effective operation may be achieved by optimizing these parameters. In the most common type of a heat exchanger, one fluid flows through a package of tubes, and the other around those tubes, thus exchanging heat through pipe walls.

If the fluid flowing around the tubes is in gaseous state, thermal resistance on this side of the heat exchanger is larger. The reason for the difference in heat resistance of liquid fluid and gaseous fluid sides in the heat exchanger lies in the very different physical properties of gases and liquids, namely

[*] Corresponding author. Tel.: +38591/508-8622
E-mail address: mpercic@riteh.hr

thermal capacity, thermal conductivity, kinematic viscosity, etc. The larger heat resistance on gaseous fluid side must be compensated with sufficiently enlarged heat transfer surface on that side of the heat exchanger. In practice, that means adding fins of various sizes and geometries around the pipes. Fins can be shaped in a plate or annular form, and this is the main difference between plate finned heat exchangers and annular finned heat exchangers. The liquid fluid side of the heat exchanger, i.e. tubes, can be arranged in an in-line or cascade formation. The cascade formation of tubes forces the gaseous fluid to flow around them with changes in the flow direction, which enables better mixing of fluid particles, and longer passages through the heat exchanger, hence the heat transfer is increased. Moreover, the tubes can have a circular or flat shaped cross section. These sorts of heat exchangers constitute a large group of fin-and-tube heat exchangers. Many papers describe numerical and experimental investigations of fin-and-tube heat exchangers. Numerical analysis of an annular finned tube heat exchanger is described in [1], where the section of a heat exchanger with one fin is simulated for various operating and geometric variables. Another numerical investigation studies and compares the air-side model with the air/water-side model of a plain fin-and-tube heat exchanger in [2]. The analysis of heat transfer in the fin-and-tube heat exchanger with wavy fins is described in [3]. Numerical investigations with various fin geometries are exhibited in [4], [5], [6], [7] and [8]. Experimental measurements on fin-and-tube heat exchangers which are then used for numerical validation are described in [9], [10] and [11]. Also, the infrared thermography can be used to experimentally determine temperature distributions in a heat exchanger, which is described in [12]. Studying the flow field on the gaseous side of a heat exchanger with louvered fins is described in [13]. The thermal contact resistance of a fin to tube attachment is analyzed in [14]. A significant contribution to this research field includes a three dimensional numerical analysis of turbulent fluid flow so that heat transfer on the air-side and water-side is performed, with non-constant physical properties. In order to obtain the heat transfer characteristics of plain fin-and-tube heat exchangers, a numerical method enabling the simulation of all the fins of two analyzed heat exchangers is employed, i.e. the whole heat exchangers are simulated.

2 Heat exchanger design

Both types of heat exchangers analyzed in this paper are of plain fin-and-tube type with flat tubes. The type with cascade flat tube arrangement in three rows is of the heat exchanger surface type 9.1-0.737-S according to [15], and the in-line flat tube arrangement in two rows type is of the heat exchanger surface type 9.68 - 0.870. Both heat exchangers are designed using the selection method and experimental Colburn j-factor data from the [15]. The geometries of both studied heat exchanger geometries are shown in Fig. 1. and Table 2.
The selection and dimensioning of the heat exchangers are done for the input parameters of water and air (temperatures and velocities), and required heat load. Both heat exchangers are selected using the same input parameters and required heat load. The used input parameters are shown in the Table 1. For both heat exchangers, the fins are made of aluminum and flat tubes of copper. The fin thickness is 0.1 mm and tube wall thickness is 0.2 mm.

3 The mathematical model

The mathematical model of both heat exchangers is comprised of computational domain, governing equations and boundary conditions. The mathematical model describes heat transfer between two fluids in the heat exchangers. The heat transfer process includes convective heat transfer from warmer fluid (water) to the pipe wall surface, conduction of heat through the pipe wall, and then the heat from the pipe wall is in part transferred by convection on the flowing air, and in part by conduction on to the fin. The heat from the fin is also transferred by convection on to the flowing air. This heat transfer mechanism which occurs inside the heat exchanger is completely simulated as a conjugated numerical method, including conduction through pipe walls and fin, and convection on the air and water sides of the heat exchanger. The assumptions of the mathematical model are constant density of fluids (air and water) and constant density and specific heat capacity of solids (copper and aluminum). All other physical properties which

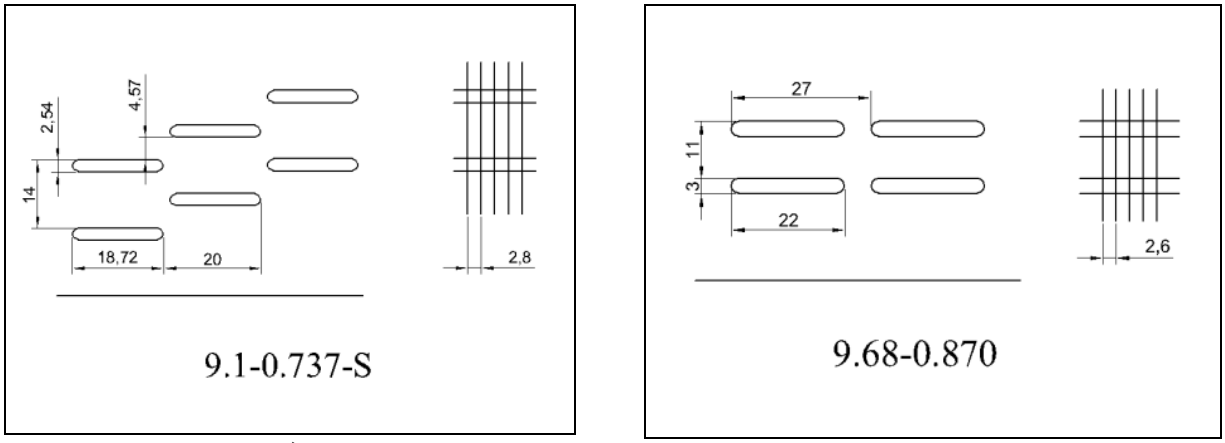

a) b)

Figure 1. Geometries of studied plain fin-and-tube heat exchangers [15]: a) with cascade flat tube arrangement in three rows, and b) with in-line flat tube arrangement in two rows.

Table 1. Input parameters for selection and dimensioning of both studied heat exchangers.

Calculation parameter	Air	Water
Inlet temperature [°C]	30	100
Outlet temperature [°C]	55	90
Inlet velocity [m/s]	10	0.6
Heat load [kW]	35	

Table 2. Selected dimensions of both studied heat exchangers.

Dimension	Cascade tube arr.	In-line tube arr.
Height [m]	0.21	0.165
Length [m]	0.686	0.986
Width [m]	0.1	0.1
Number of fins	237	365
Number of tubes	35	25
Heat exch. surface [m^2]	10.587	12.32

have relatively high rate of change with temperature are considered as non-constant, these properties being dynamic viscosity (η), thermal conductivity (λ) and specific heat capacity (c_p) for fluids (air and water), specific heat capacity only for solids (copper tube and aluminum fin).

3.1 The computational domain

The computational domain is divided into four sub-domains: air, water, aluminum fin, and copper pipes. The air sub-domain is a volume of air with the inlet length of 1.5 times the fin length (s = 0.1m), and the outlet length of air sub-domain is 3 times the fin length. The inlet and outlet lengths of air sub-domain are assumed long enough to have fully-developed outlet air flow from the computational domain.

The computational domain of both heat exchangers is a representative part of the heat exchanger shown in Fig. 2. (dashed lines). The domain is assumed to contain all relevant physical phenomena which recur in other equivalent heat exchanger parts. All sub-domains are modeled using dimensions of corresponding heat exchanger surfaces shown in Fig. 1.

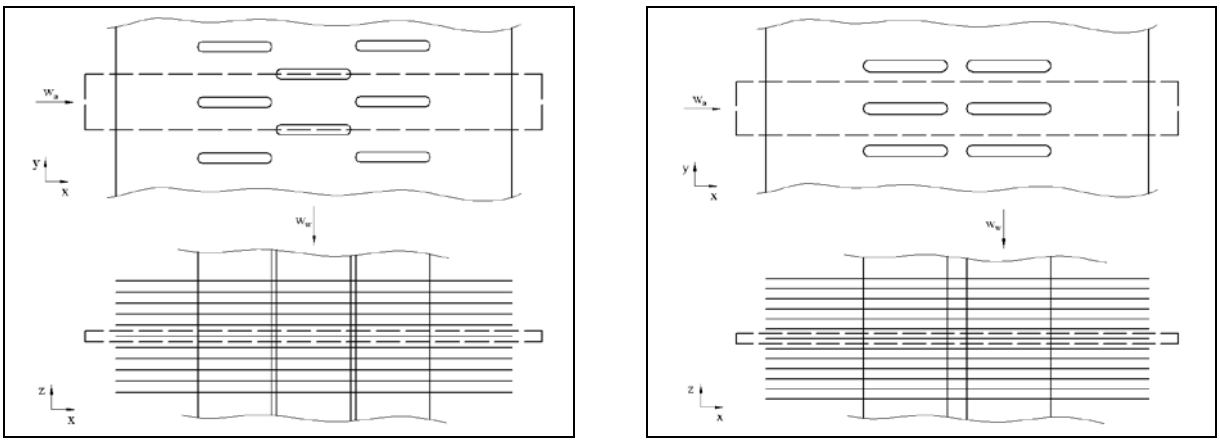

a) b)

Figure 2. Computational domain of heat exchangers: a) cascade arrangement, and b) in-line arrangement.

3.2 Governing equations

The modeled problem is a 3D, steady, turbulent, incompressible fluid flow and heat transfer. The turbulent model used is a standard *k-ε* model which is described by two differential equations: turbulent kinetic energy (*k*) and turbulence dissipation rate (*ε*). The differential equations describing physical phenomena in fluid sub-domains (air and water) are: continuity equation, momentum equations, energy equations, turbulent kinetic energy and turbulence dissipation rate. The differential equation describing heat transfer in solid sub-domain (copper tubes and aluminum fin) is the energy equation. All equations are displayed below for both fluid and solid sub-domains.

Fluid sub-domains (air and water):

▪ Continuity equation:

$$\frac{\partial(\rho \cdot w_x)}{\partial x} + \frac{\partial(\rho \cdot w_y)}{\partial y} + \frac{\partial(\rho \cdot w_z)}{\partial z} = 0\,. \tag{1}$$

▪ Momentum equations:

x axis direction:
$$\rho \cdot \left(w_x \frac{\partial w_x}{\partial x} + w_y \frac{\partial w_x}{\partial y} + w_z \frac{\partial w_x}{\partial z} \right) = -\frac{\partial p}{\partial x} + \eta \cdot \left(\frac{\partial^2 w_x}{\partial x^2} + \frac{\partial^2 w_x}{\partial y^2} + \frac{\partial^2 w_x}{\partial z^2} \right). \tag{2}$$

y axis direction:
$$\rho \cdot \left(w_x \frac{\partial w_y}{\partial x} + w_y \frac{\partial w_y}{\partial y} + w_z \frac{\partial w_y}{\partial z} \right) = -\frac{\partial p}{\partial y} + \eta \cdot \left(\frac{\partial^2 w_y}{\partial x^2} + \frac{\partial^2 w_y}{\partial y^2} + \frac{\partial^2 w_y}{\partial z^2} \right). \tag{3}$$

z axis direction:
$$\rho \cdot \left(w_x \frac{\partial w_z}{\partial x} + w_y \frac{\partial w_z}{\partial y} + w_z \frac{\partial w_z}{\partial z} \right) = -\frac{\partial p}{\partial z} + \eta \cdot \left(\frac{\partial^2 w_z}{\partial x^2} + \frac{\partial^2 w_z}{\partial y^2} + \frac{\partial^2 w_z}{\partial z^2} \right). \tag{4}$$

▪ Energy equation:

$$\rho \cdot \left(w_x \frac{\partial T}{\partial x} + w_y \frac{\partial T}{\partial y} + w_z \frac{\partial T}{\partial z} \right) = \frac{\lambda}{c_p} \cdot \left(\frac{\partial^2 T}{\partial x^2} + \frac{\partial^2 T}{\partial y^2} + \frac{\partial^2 T}{\partial z^2} \right). \tag{5}$$

▪ Turbulent kinetic energy:

$$\frac{\partial(\rho \cdot k \cdot u_i)}{\partial x_i} = \frac{\partial}{\partial x_j}\left[\left(\eta + \frac{\eta_t}{\sigma_k}\right)\frac{\partial k}{\partial x_j}\right] + G_k + G_b - \rho \cdot \varepsilon - Y_M + S_k \,. \tag{6}$$

Turbulence dissipation rate:

$$\frac{\partial(\rho \cdot \varepsilon \cdot u_i)}{\partial x_i} = \frac{\partial}{\partial x_j}\left[\left(\eta + \frac{\eta_t}{\sigma_\varepsilon}\right)\frac{\partial \varepsilon}{\partial x_j}\right] + C_{1\varepsilon}\frac{\varepsilon}{k}\left(G_k + C_{3\varepsilon}G_b\right) - C_{2\varepsilon}\frac{\rho \cdot \varepsilon^2}{k} + S_\varepsilon \,. \tag{7}$$

Solid sub-domains (copper tubes and aluminum fin):

▪ Energy equation:

$$\frac{\lambda}{c_p} \cdot \left(\frac{\partial^2 T}{\partial x^2} + \frac{\partial^2 T}{\partial y^2} + \frac{\partial^2 T}{\partial z^2}\right) = 0 \,. \tag{8}$$

3.3 Boundary conditions

The boundary conditions define the values of variables on the boundary planes of the computational domain. The computational domain is defined on its boundaries as follows. The inlet air plane on the air sub-domain is defined as velocity-inlet boundary condition, where the inlet air velocity and temperature are kept constant. The inlet water plane inside the copper pipes is also defined as a velocity inlet boundary condition, where inlet water velocity and temperature are kept constant. The fluid outlet planes are defined with a zero-gradient boundary condition, where a fully-developed flow of both water and air is assumed. The planes of the computational domains which represent the boundaries from the rest of the heat exchanger are set as symmetry boundary conditions, because the neighboring geometry is mirrored and the temperature and flow fields are symmetrical. The planes of contact between solid and fluid sub-domains are defined with an interface boundary condition which comprises zero-velocity of fluid and equally exchanged heat-flux. The boundary conditions for both heat exchangers are shown in Fig. 3., and in continuance the mathematical definitions of all boundary conditions are given.

4 The numerical method

The numerical method used for solving the presented mathematical model is the control volume method [16]. The discretisation scheme used is a first-order upwind scheme for all equations except energy equation which was discretised with a second-order upwind scheme. The numerical simulation has been done with commercial software *Fluent* The calculation domain has been modelled and meshed using software *Gambit*. Both analyzed heat exchanger geometries were modeled with a non-conformal mesh, in a way that all sub-domains were meshed independently with optimum size and shape of the control volumes. Only the meshes of the fin sub-domains are shown for clarity in Fig. 4 as the cascade tube arrangement (a), and in-line tube arrangement (b) geometries. The high-gradient zones of all sub-domains were meshed using the size-functions in order to obtain high density of mesh in areas of high rate of change of variables. To ensure proper heat conduction simulation, the pipe walls were meshed with three control volumes per pipe wall thickness (0.2 mm), and on the fin sub-domain with at least two control volumes per fin thickness (0.1 mm). All sub-domains were joined together with an interface boundary condition to ensure correct heat transfer calculation between them. The meshes of both heat exchangers were tested for quality in *Gambit* and *Fluent*, and good quality of all meshes is achieved. The quality of geometry control volume is approved with the following tests: aspect ratio tests of geometry control volume boundaries, equisize skew tests which are normalized measures of skewness for control volumes, and volume tests to assure no negative volumes are present in the meshes. The boundary layers of both air and water sub-domains were modeled in order to obtain a good turbulent flow simulation and values of dimensionless wall distance y^+ are kept in recommended values, below y^+=1. For both models of heat exchangers, the grid independency test has been done. For the heat exchanger with cascade tube arrangement, the

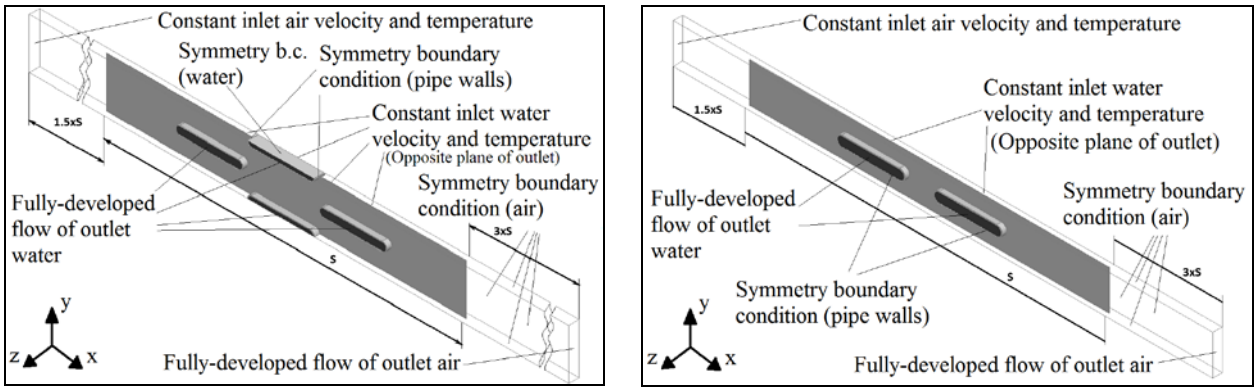

Figure 3. Boundary conditions of computational domain of heat exchangers: a) a cascade arrangement, and b) an in-line arrangement.

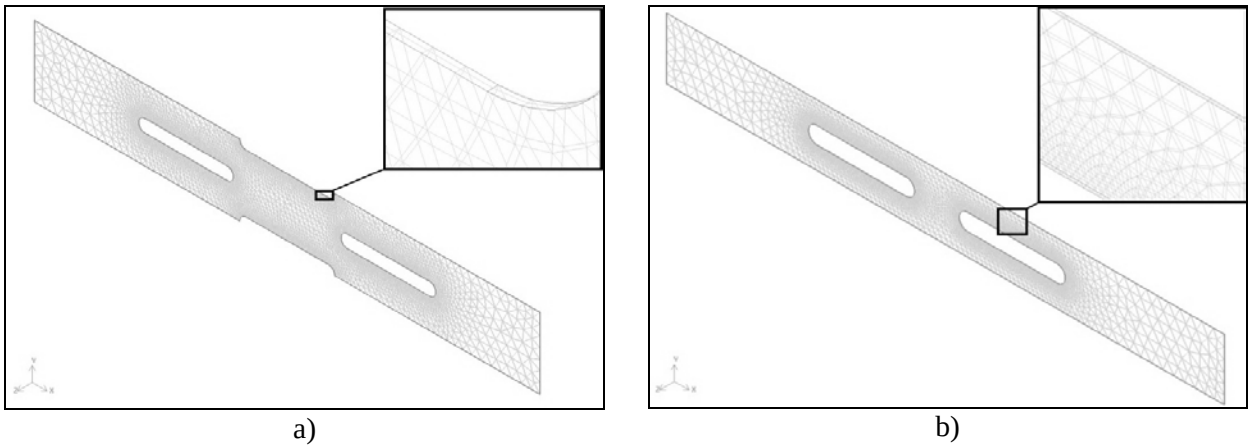

Figure 4. The meshes of the fin sub-domains: a) for the cascade tube arrangement, and b) in-line tube arrangement geometries.

computational domain consisting of 191 032 control volumes has met the independency test requirements, and for the heat exchanger with in-line tube arrangement, the computational domain consists of 247 556 control volumes. The turbulence model used with *Fluent* is a standard *k-ε* turbulence model, being widely approved and recommended in literature for the relatively low *Re* numbers involved in the simulated cases. The simulations were not tested with other turbulence models due to the lack of experimental data for the tested heat exchangers so that validation would be impossible. The input values for this turbulence model are turbulence intensity (*I*) calculated by the equation (9), and the hydraulic diameter (d_h).

$$I = 0.16 \cdot \mathrm{Re}_{dh}^{2/3} \ [\%]. \qquad (9)$$

The input values for *k-ĺ* turbulence model for both heat exchangers are displayed in Table 3.

The standard wall functions, most widely used in industrial applications, have been also used in *Fluent*, whereas testing of other wall functions to make the appropriate model evaluation has not been done again because of the lack of experimental data.. The numerical simulation given in this paper takes into account all of the fins of both heat exchangers. All fins are simulated in order to get the outlet water temperature from the crossflow heat exchanger, as well as temperature distributions of air and water. All fins are simulated in a way that the first fin (the fin at the water inlet) is simulated with water inlet parameters, and after the solution has been converged, the temperature, velocity profile, *k* and *ĺ* values on outlet water boundary are stored. Afterwards, all saved data from the water

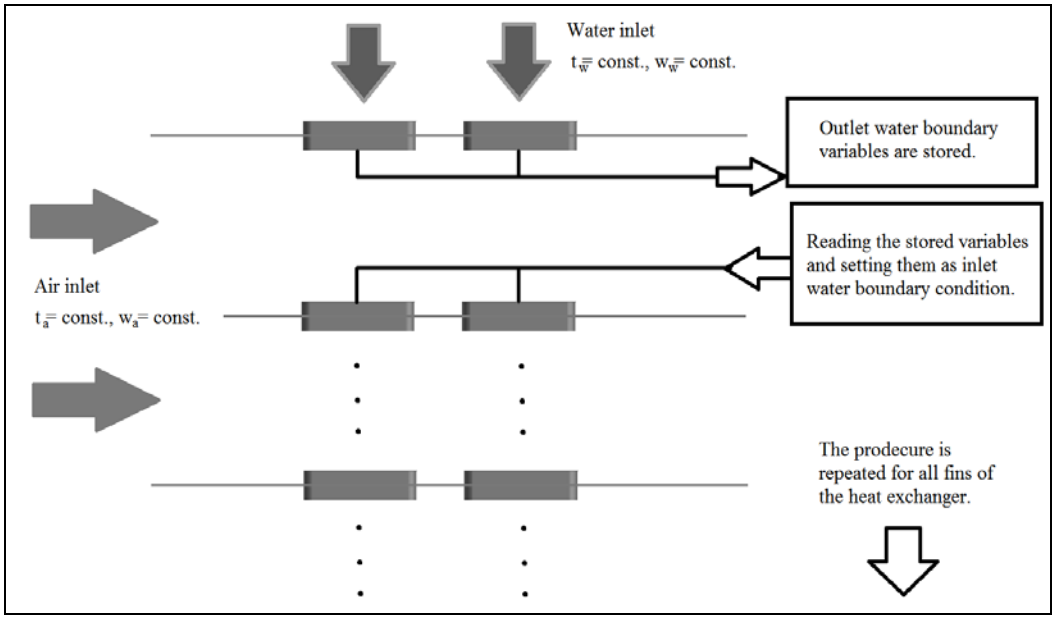

Figure 5. A schematic representation of the calculation procedure used for all the fins of the heat exchanger.

Inlet boundary conditions:

- Air inlet plane:

$$w_x = w_a, w_y = 0, w_z = 0.$$
$$T_{in} = T_{a-in}.$$

- Water inlet plane:

$$w_x = 0, w_y = 0, w_z = w_w.$$
$$T_{in} = T_{w-in}.$$

Outlet boundary conditions:

- Air outlet plane:

$$\frac{\partial w_x}{\partial x} = 0, \frac{\partial w_y}{\partial x} = 0, \frac{\partial w_z}{\partial x} = 0, \frac{\partial T_a}{\partial x} = 0.$$

- Water outlet plane:

$$\frac{\partial w_x}{\partial z} = 0, \frac{\partial w_y}{\partial z} = 0, \frac{\partial w_z}{\partial z} = 0, \frac{\partial T_w}{\partial z} = 0.$$

Symmetry boundary conditions:

- Air sub-domain:

$$\frac{\partial w_x}{\partial z} = 0, \frac{\partial w_y}{\partial z} = 0, w_z = 0, \frac{\partial T_a}{\partial z} = 0.$$
$$\frac{\partial w_x}{\partial z} = 0, \frac{\partial w_z}{\partial z} = 0, w_y = 0, \frac{\partial T_a}{\partial z} = 0.$$

- Water sub-domain (only for heat exchanger with cascade tube arrangement):

$$\frac{\partial w_x}{\partial y} = 0, \frac{\partial w_z}{\partial y} = 0, w_y = 0, \frac{\partial T_w}{\partial y} = 0.$$

- Copper pipe sub-domain:

$$\frac{\partial T_p}{\partial z} = 0, \frac{\partial T_p}{\partial y} = 0.$$

- Aluminum fin sub-domain:

$$\frac{\partial T_f}{\partial y} = 0.$$

Interface boundary conditions:

- Air – fin interface:

$$\lambda_a \frac{\partial T_a}{\partial n} = \lambda_f \frac{\partial T_f}{\partial n}.$$

- Air – pipes interface:

$$\lambda_a \frac{\partial T_a}{\partial n} = \lambda_p \frac{\partial T_p}{\partial n}.$$

- Water – pipes interface:

$$\lambda_w \frac{\partial T_w}{\partial n} = \lambda_p \frac{\partial T_p}{\partial n}.$$

Table 3. Input values for k-ε turbulence model.

	Cascade arr.		In-line arr.	
Value	**Water**	**Air**	**Water**	**Air**
I [%]	5.5	6	5.1	5.93
d_h [m]	0.00415	0.0048	0.0046	0.00433

Table 4. Validation results for computational time decreasing method of numerical simulation.

Simulation	$t_{w\text{-}out}$ [°C]	$t_{a\text{-}out}$ [°C]
With initialization	89.58	56.71
Without initialization	89.2	56.77

Table 5. Studied cases of different inlet air velocities and temperatures.

Case	$t_{a\text{-}in}$ [°C]	$w_{a\text{-}in}$ [m/s]
1	5	10
2	5	20
3	30	10
4	30	20

outlet boundaries are set as inlet water variables for the next fin - domain. This process has been made to run automatically by a specially written script. The calculation process is schematically shown in Fig. 5. All other fins of the heat exchangers after the first one have been simulated without initialization of variables in *Fluent*. To reduce needed computational time, the following fin simulations have been done without using the initialization with neglectable solution differences. This method of calculation time reduction is numerically and physically sound because the flow and temperature fields of neighboring fins are very similar, and without using variable initialization the time needed for achieving convergence is greatly reduced for consequent fins. This method has been validated by running a simulation run of all fins with initialization on a super-computer, and comparing the results obtained from a simulation without consequent fin variable initialization. The values of average outlet air and water temperature have been compared from both simulation runs. The difference between obtained results is acceptable considering a noticeable decrease in computational time, which was from roughly 3 hours needed for one fin to about 3.5 hours needed for all fins. The results obtained are shown in Table 4. All the numerical simulations of both analyzed heat exchangers in this paper have been done using this method for all tested cases.

5 The results

The numerical analysis consists of simulation runs for all fins of both studied heat exchangers for four different cases of inlet air velocity and temperatures. The inlet air variables for four cases are shown in Table 5. The water inlet velocity and temperature is kept constant in all studied cases. Variable data for all fins of both heat exchangers for all studied cases has been stored and processed. To keep this paper concise, only the temperature distribution on fin surface is shown.

The results were obtained by using the following expressions for calculation:

- Colburn j-factor:

$$\mathrm{j} = \mathrm{St} \cdot \mathrm{Pr}^{2/3}. \tag{10}$$

- Prandtl number:

$$\mathrm{Pr} = \frac{\eta \cdot c_p}{\lambda}. \tag{11}$$

▪ Reynolds number:

$$\mathrm{Re} = \frac{\rho \cdot w \cdot d_e}{\eta}. \qquad (12)$$

▪ Nusselt number:

$$\mathrm{Nu} = \frac{\alpha \cdot d_e}{\lambda}. \qquad (13)$$

▪ Water-side convective heat transfer coefficient:

$$\alpha_w = \frac{\lambda_w}{d_{ew}} \cdot Nu_w \quad \left[\mathrm{W/m^2K}\right]. \qquad (14)$$

▪ Air-side convective heat transfer coefficient:

$$\alpha_a = St \cdot w_a \cdot \rho_a \cdot c_{p-a} \quad \left[\mathrm{W/m^2K}\right]. \qquad (15)$$

▪ Overall heat transfer coefficient:

$$\frac{1}{k} = \frac{1}{\alpha_w \cdot \frac{A_r}{A_e}} + \frac{1}{\alpha_a \cdot \eta_0} \quad \left[\mathrm{m^2K/W}\right]. \qquad (16)$$

▪ Finned surface efficiency:

$$\eta_0 = 1 - \frac{A_a}{A_e} \cdot (1 - \eta_\alpha). \qquad (17)$$

Where the η_α coefficient is calculated as:

$$\eta_\alpha = \frac{\tanh\left(m \cdot \frac{t_1 - b}{2}\right)}{\left(m \cdot \frac{t_1 - b}{2}\right)}. \qquad (18)$$

And the factor *m* is:

$$m = \sqrt{\frac{2 \cdot \alpha_a}{\lambda_f \cdot \delta_f}}. \qquad (19)$$

The finned surface efficiency of the heat exchangers calculated from the expression (17) depends on the geometry characteristics which are taken into account with the coefficient η_α (18) and the factor *m* (19). The geometry characteristics (t_1 and *b)* which influence the finned surface efficiency in the expression (18) are shown in Fig. 6. Also the thermal conductivity of the fin material λ_f and the fin thickness δ_f influence the fin efficiency through the factor *m* (19).

5.1 Temperature distributions

Additionally, the effect of various inlet air temperatures and velocities on fluid flow and heat transfer inside the heat exchanger was elaborated. The calculated temperature fields on a fin surface of the heat exchanger with a cascade tube arrangement (120^{th} fin) used in different cases are displayed for all studied cases in Fig. 7. The heat is conducted from the tube wall to the fin, and the highest temperatures are evident in those regions of the fin-tube contact. The heat dissipates on to the flow of air over the fin which cools the fin surface; hence the lower temperatures are evident further away from tube-fin contacts. The lower inlet air velocities have resulted in higher temperatures across the fin surface because of lower heat transfer to the inflowing air as a result of lower mixing rates of fluid layers. The temperature of the inflowing air also greatly affects the heat transfer inside the heat exchanger. For tested cases with higher temperature of inflow air (cases 3 and 4), the fin surface temperature distributions are evidently higher, which results in lower heat transfer rate due to lower temperature differences of the air flow and fin surface. The overall fin temperature affects the air-side heat transfer α_a (15), and also the fin efficiency η_0 (17) through the factor *m* (19). Higher fin efficiency is obtained with lowest inlet air temperature and highest inlet air velocity, which is evident by lowest overall fin surface temperatures, this combination of inlet air temperature and velocity is studied as case 2., and it is visible in Fig. 7., that for that case, the temperatures of the fin surface are the lowest. By contrast/in contrast to this, the higher inflow air temperatures and lower inlet velocities, studied in case 3, have a diminishing effect on heat transfer and higher overall fin temperatures where the fin efficiency is lowest, which is evident in Fig. 7., by higher temperatures of fin surface area. The heat transfer is lowest for this case due to the lower temperature differences of the fin surface and the inflowing air, and the low inlet speed of air is insufficiently

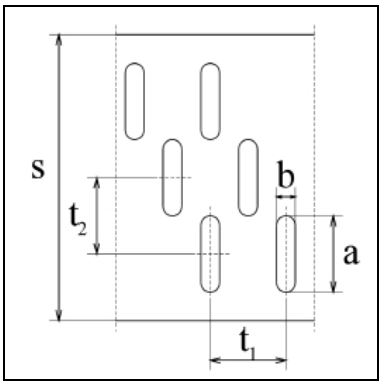

Figure 6. Geometry characteristics influencing fin efficiency.

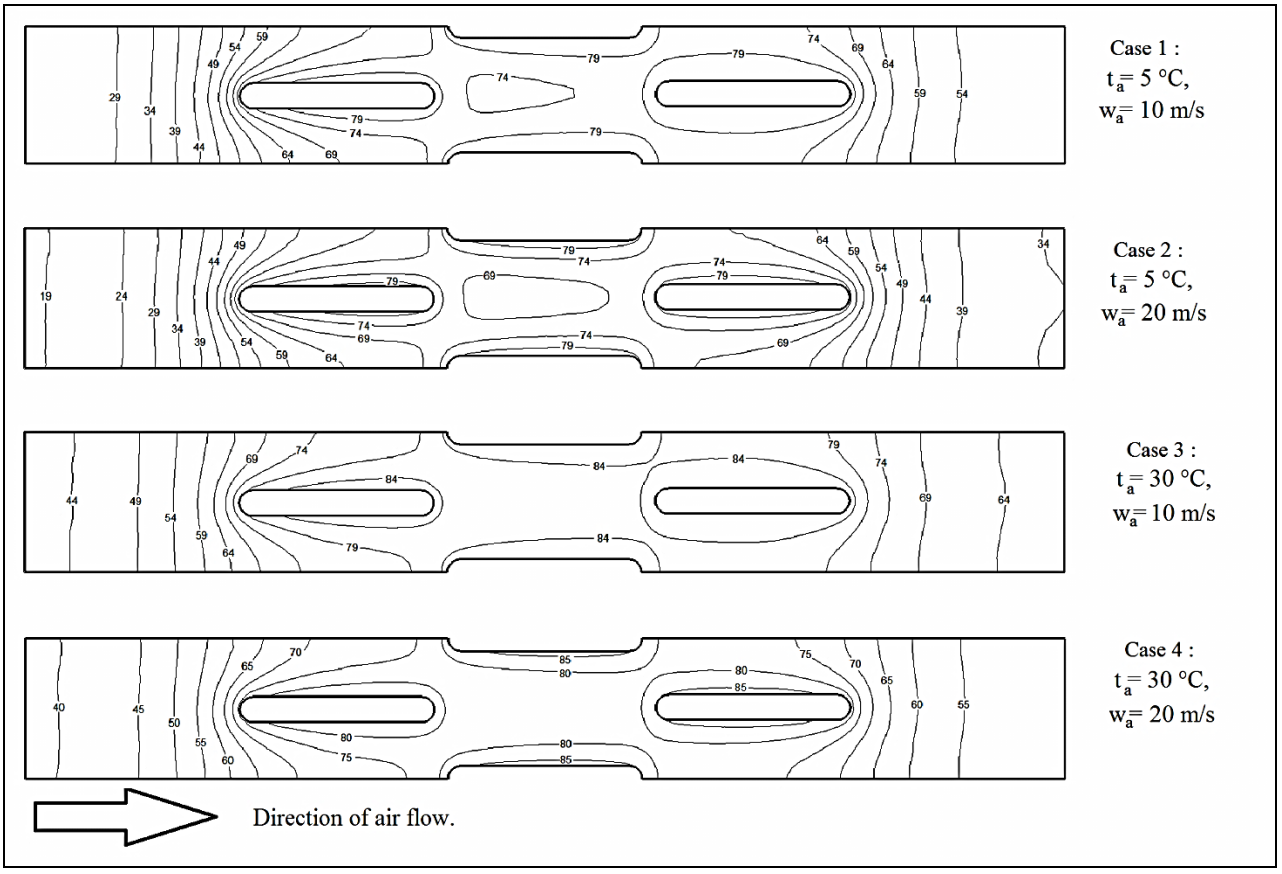

Figure 7. Isotherms showing temperature distribution over fin surface of the analyzed heat exchanger with a cascade tube arrangement for all studied cases (°C).

turbulent to intensify the mixing of air layers. The calculated temperature distributions on the fin surface of the studied heat exchanger with an in-line tube arrangement (200th fin) are displayed in Fig. 8. The temperature distributions are complying with physical expectations and are evidently in accordance with the previously explained results of the heat exchanger with a cascade tube arrangement. It is also visible below that the low inlet air temperature results in lower temperatures across the fin surface. Higher inlet air velocities result in lower temperatures across the fin surface, which is analog to results for a heat exchanger with a cascade tube arrangement. Also for this geometry of a fin-and-tube heat exchanger, it is evident that the higher heat transfer rate and fin efficiency is

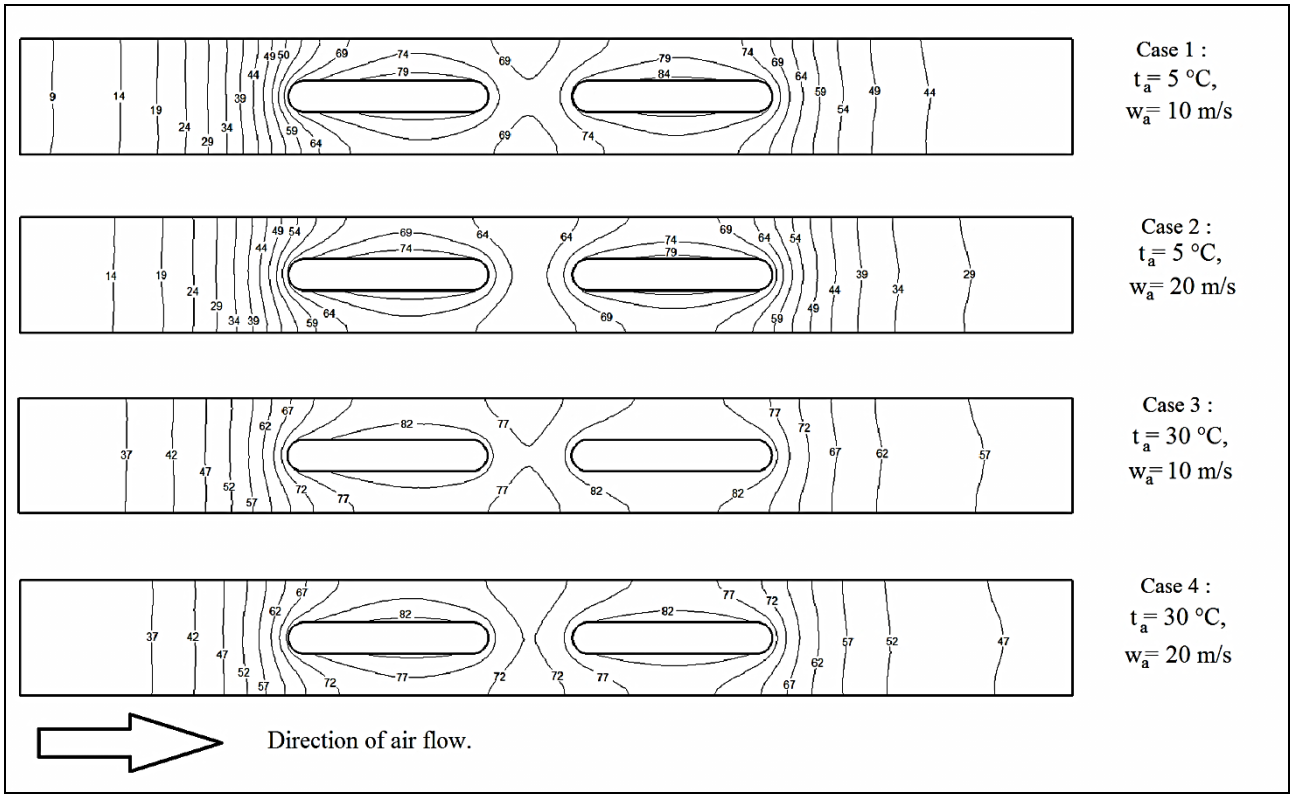

Figure 8. Isotherms showing temperature distribution over the fin surface of the analyzed heat exchanger with an in-line tube arrangement for all studied cases (°C).

achieved with the lowest inlet air temperatures and highest inlet air velocities. The highest fin surface temperatures, i.e. lowest heat transfer rate and fin efficiency, are visible for the case 3 where the inlet air temperature is high, and inlet air velocity is low. It can also be noticed for both heat exchanger geometries that the isotherms are concentrically expanding from tube-fin contact areas of the fins, which is a result of heat conductance from the tube wall to the fin. The isotherm lines are visually 'swept' in the direction of the inflowing air which is the result of the heat transfer by convection to the air flow. The temperature fields around the tube-fin contacts that are positioned further away from the air inlet are showing higher temperatures, because the air which flows over those parts of the fin has already been heated up at the upwind tube. As a result the heat transfer rate and fin efficiency in the part of the fin near the air outlet is lower than in the near-intake part of the fin. It must also be mentioned that the heat flow on to the inflowing air does not only come from the fin heated by the tube walls through tube-fin contacts, but also from the tube walls which are exposed to the inflow air between the fins.

5.2 Heat transfer characteristics

The calculated values of heat transfer characteristics for all the fins of the heat exchanger are displayed in diagrams in function of number of fins, i.e. heat transfer surface in the water flow direction. The values calculated are the outlet temperatures of water and air, convective heat transfer coefficients of water and air, the Nusselt number, the Colburn j-factor, and the overall heat transfer coefficient. The heat transfer characteristics of a heat exchanger with a cascade tube arrangement are displayed in Figs. 9. and 10. In Table 6., the average values of heat transfer characteristics are given in comparison with values obtained by analytical methods from literature [15], for the analyzed case with inlet air velocity of 10 m/s and inlet air temperature of 30 °C (case 3). Good agreement of the majority of values can be observed. In Figs. 10a and 10b, the outlet temperature values of air and temperature of water are displayed. It is evident that the outlet air temperature is greater for cases with higher inlet air temperatures and diminishes in the cases with higher inlet air velocity. The outlet air flow temperature has lower values for fins near the water

Table 6. Average values of heat transfer characteristics of a heat exchanger with cascade tube arrangement.

	$t_{w\text{-}out}$ [°C]	α_w [W/m^{2}K]	α_a [W/m^{2}K]	j	Nu	k [W/m^{2}K]
Numerical	89.2	6035.34	82.06	0.0053	34.88	63.65
Analytical	90	6071	81.36	0.0053	35	63.31

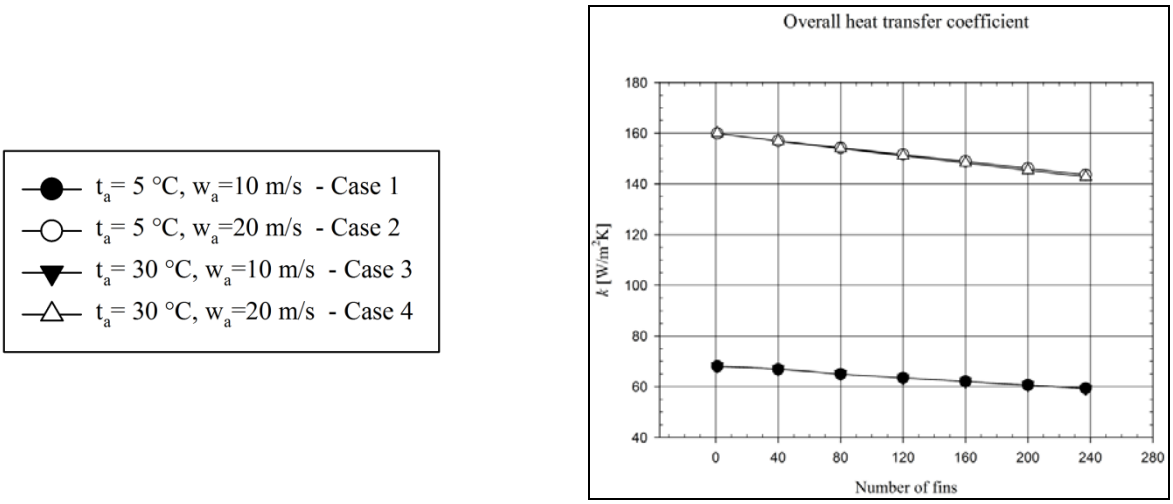

Figure 9. Overall heat transfer coefficient of the analyzed heat exchanger with cascade tube arrangement.

outlet, which is the result of a lower heat transfer due to the smaller temperature difference between water and air. The diminishing air-side heat transfer also results in lower fin efficiency for subsequent fins. As a result of lower fin efficiencies, the overall heat transfer coefficient also falls for subsequent fins, as visible in Fig. 9. The values of outlet water temperature agree with the physical observations mentioned earlier, i.e. outlet water temperature is highest for the case with the highest inlet air temperature and lowest inlet air velocity. The air-side convective heat transfer coefficient values displayed in Fig. 10c show higher values for the cases with higher inlet air velocities which results in favorable higher turbulence of the air flow. The values of convective air heat transfer coefficient show great differences for cases with different air inlet velocities, and inlet air temperature shows no noticeable effect on the air-side convective heat transfer coefficient. Also there is no noticeable effect of inlet air temperature on Colburn j-factor values.

The variables of heat transfer characteristics for the analyzed heat exchanger with an in-line tube arrangement are displayed in Figs. 11. and 12. The average values of heat transfer variables are compared to the analytical values gained from calculations, and are displayed in Table 7. The agreement of most values in Table 7. are good, but there is more discrepancy between the values when compared to the values of the heat exchanger with a cascade tube arrangement. The overall heat transfer coefficient for all cases for the heat exchanger with an in-line tube arrangement has lower values compared to the heat exchanger with a cascade tube arrangement. The reason for this is that the cascade tube arrangement enables better mixing of air layers and a more turbulent flow when compared to the heat exchanger with an in-line tube arrangement. This is also visible when observing the convection heat transfer coefficient for air. The air-side convective heat transfer coefficients in Fig. 12c also show no change with different inlet air temperatures, which can also be observed for the Colburn j-factor. The Nusselt number values are also greater for the cases with lower inlet air temperatures. The similarity of diagrams with the Nusselt number and water-side convection heat transfer coefficient lies in the linear dependency of the Nusselt number and convective heat transfer coefficient.

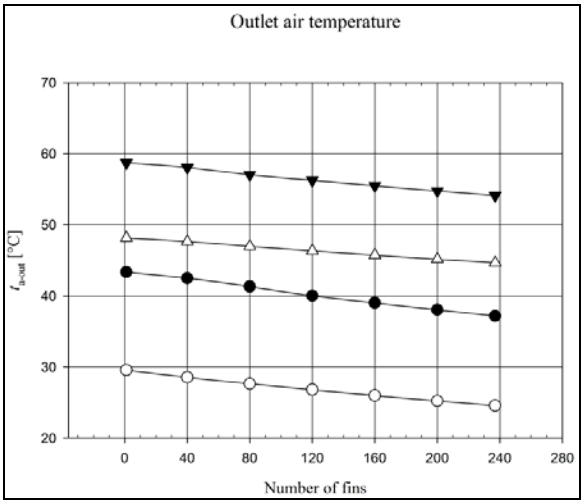

a)

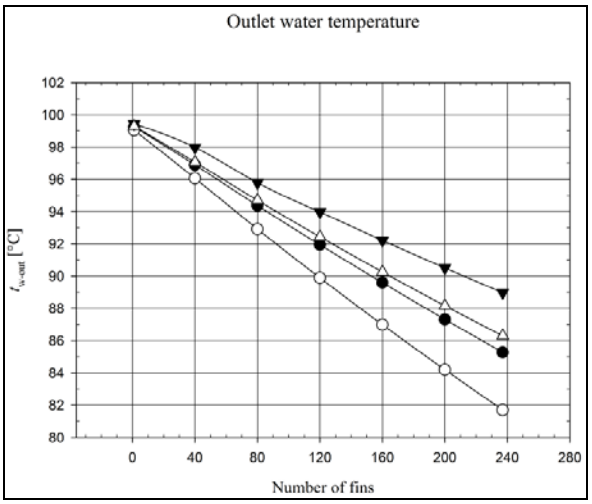

b)

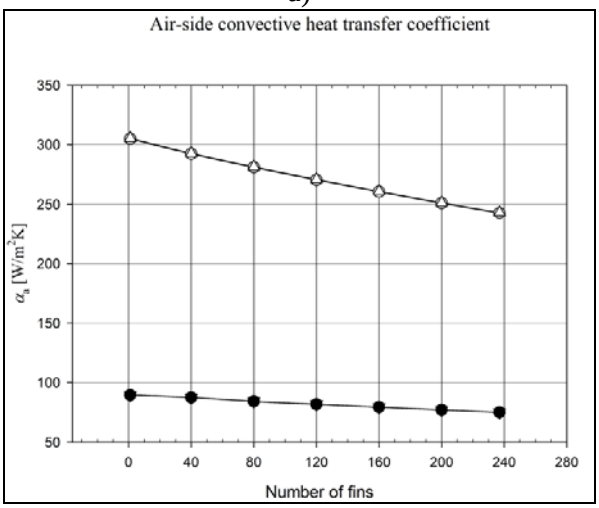

c)

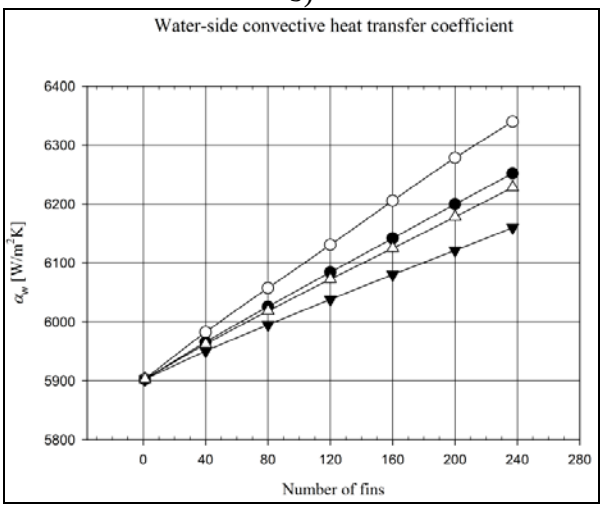

d)

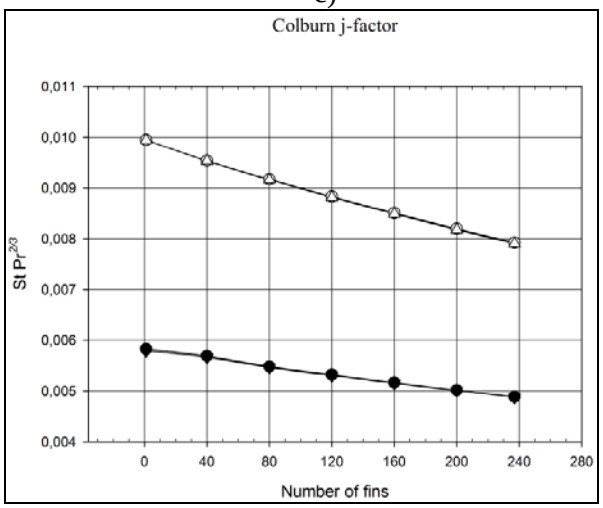

e)

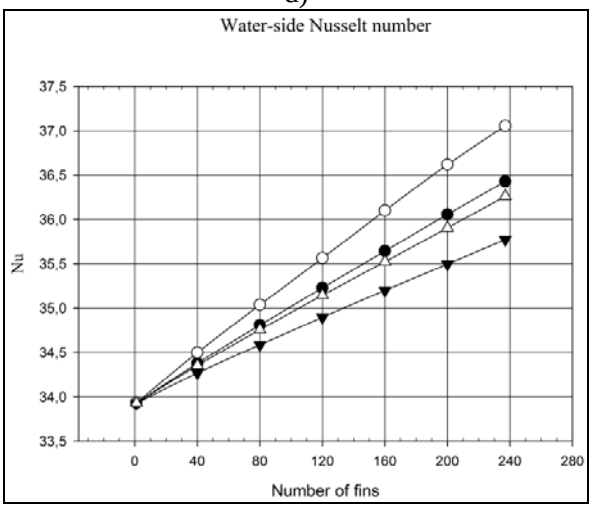

f)

Figure 10. Heat transfer characteristics of the heat exchanger with a cascade tube arr. (legend in Fig. 9).

Table 7. Average values of heat transfer characteristics of a heat exchanger with in-line tube arrangement.

	$t_{w\text{-}out}$ [°C]	α_w [W/m^{2}K]	α_a [W/m^{2}K]	j	Nu	k [W/m^{2}K]
Numerical	92.21	7183.67	63.42	0.0041	49.23	57.02
Analytical	90	7179.5	59.85	0.0039	49	54.2

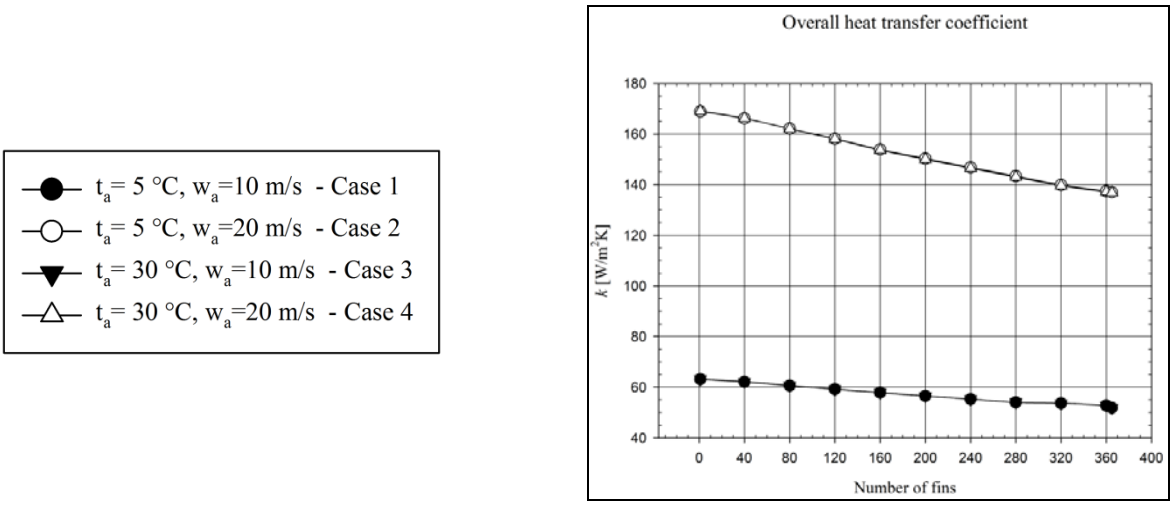

Figure 11. Overall heat transfer coefficient of the analyzed heat exchanger with an in-line tube arrangement.

6 Conclusion

Two types of plain fin-and-tube heat exchanger have been analyzed in this paper. The heat exchangers were selected using analytical methods from the literature. Both heat exchangers where numerically simulated with non-constant physical properties for four cases of inlet air velocities and temperatures. A special numerical method has been used after validation to simulate all the fins of both heat exchangers, i.e. complete crossflow heat exchangers have been simulated. The used numerical procedure could be used for heat transfer and fluid flow simulations of similar crossflow heat exchangers. A number of data has been acquired from the simulation results, the paper describes temperature distributions on a fin surface of both analyzed heat exchangers for all tested cases of inlet air temperature and velocities.

The heat transfer characteristics are displayed for all tested cases for both water-side and air-side of the heat exchangers. From the displayed results it can be concluded that inlet air temperature has greater effect on heat transfer than the inlet air velocity for constant water inlet parameters. The analysis performed in this paper can provide useful data for the operating heat transfer characteristics for analyzed heat exchanger geometries. The used numerical method which enables the simulation of a complete crossflow heat exchanger with considerable computational time decrease can be used as a powerful optimization and design tool for achieving the largest possible value of heat exchanger effectiveness.

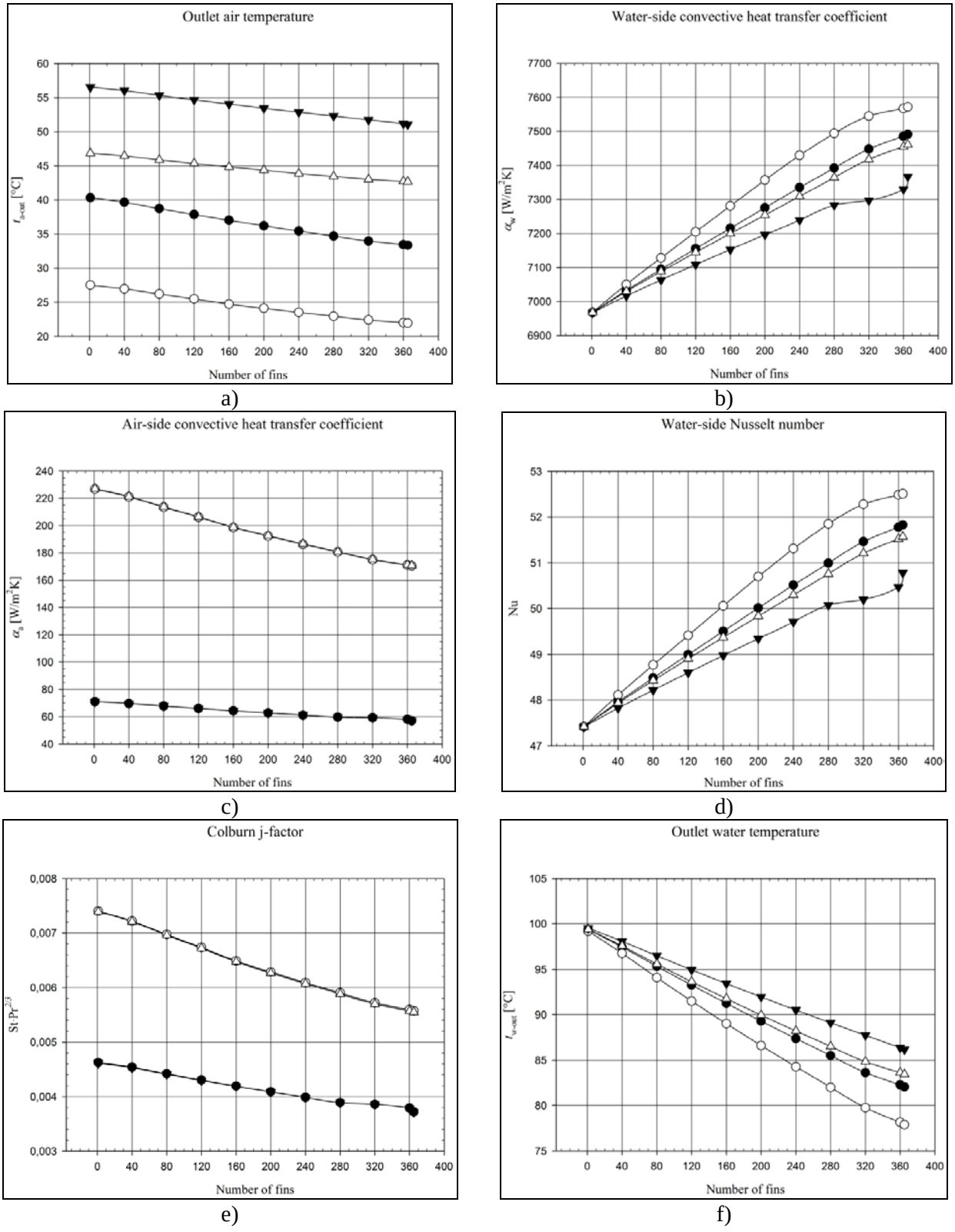

Figure 12. Heat transfer characteristics of the heat exchanger with in-line tube arr. (legend in Fig. 11).

7 List of symbols

A_a, m^2	finned surface area
A_e, m^2	air-side heat transfer area
A_r, m^2	water-side heat transfer area
c, J/kgK	specific heat capacity
C	constant
d, m	diameter
G_k	generation of turbulence kinetic energy due to the mean velocity gradient
G_b	generation of turbulence kinetic energy due to buoyancy
I, %	turbulence intensity
j	Colburn j-factor
k, W/m^{2}K	overall heat transfer coefficient
	turbulence kinetic energy
Nu	Nusselt number
p, Pa	pressure
Pr	Prandtl number
Re	Reynolds number
s, m	lenght of fin
S	source terms
St	Stanton number
T, K	absolute temperature
t, °C	relative temperature
u, m/s	fluctuating velocity component
w, m/s	velocity
x, y, z	Cartesian coordinates
Y_M	contribution of the fluctuating dilatation in compressible turbulence to the overall dissipation rate
y^+	dimensionless wall distance
α, W/m^{2}K	convective heat transfer coefficient
δ, m	fin thickness
ε	rate of dissipation
σ	turbulent Prandtl number
ρ, kg/m^3	density
η, Pas	dynamic viscosity
λ, W/mK	thermal conductivity

Indexes:

a	air
f	fin
w	water
in	inlet
out	outlet
k	value for k
ε	value for ε
h	hydraulic
dh	value for hydraulic diameter

References

[1] Senčić, T., Trp, A., Lenić, K.: *Parametarska analiza utjecaja pogonskih uvjeta i geometrijskih parametara na izmjenu topline u cijevnom izmjenjivačcu topline s prstenastim lamelama,* Engineering Review, 29 (2009), 1, 25-36.

[2] Ortega-Casanova, J., Cejudo-Lopez, J. M., Borrajo-Pelaez, R.: *A three-dimensional numerical study and comparison between the air side model and the air/water side model of a plain fin-and-tube heat exchanger,* Applied Thermal Engineering, 30 (2010), 13, 1608-1615.

[3] Franković, B., Viličić, I., Jurkowski-R., Bailly, A., Wolf, I.: *Analiza prijelaza topline na valovitom lamelnom orebrenju izmjenjivača topline,* Strojarstvo: Časopis za teoriju i praksu u strojarstvu, 46 (2004), 4-6, 137-147.

[4] Chu, P., He Y. L., Lei, Y. G., Tian, L. T., Li, R.: *Three-dimensional numerical study on fin-and-oval-tube heat exchanger with longitudinal vortex generators,* Applied Thermal Engineering, 29 (2009), 5-6, 859-876.

[5] Mitra, S. K., Bhattacharya, A., Malapure, V. P.: *Numerical investigation of fluid flow and heat transfer over louvered fins in compact heat exchanger,* International Journal of Thermal Sciences, 46 (2007), 2, 199-211.

[6] Cheah, S. C., Salim, S. M.: *Wall y+ strategy for dealing withwall-bounded turbulent flows,* Proceedings of the International Multiconference of Engineers and Computer Scientists, Hong Kong, 2009, 2165-2170.

[7] Wang, Y., Zhang, Q., Wang, L. B., Liu, Y. J., Song, K. W.: *Numerical study of the fin*

efficiency and a modified fin efficiency formula for flat tube bank fin heat exchanger, International Journal of Heat and Mass Transfer, 54 (2011),11-12, 2661-2672.

[8] Shankapal, S. R., Umesh Babu, V., Sridhara, S. N.: *CFD analysis of fluid flow and heat transfer in a single tube-fin arrangement of an automotive radiator,* Proceedings of the International Conference on Mechanical Engineering, Dhaka, Bangladesh, 2005.

[9] Glažar, V.: *Optimizacija geometrije kompaktnih izmjenjivača topline,* Doktorska disertacija, Tehnički fakultet u Rijeci 2011.

[10] Wolf, I.: *Utjecaj geometrijskih parametara na izmjenu topline i karakteristike strujanja zraka kod lamelnih izmjenjivača topline,* Magistarski rad, Tehnički Fakultet u Rijeci, 2004.

[11] Chen, J., Zhang, W., Hu, J., Dong, J.: *Experimental and numerical investigation of thermal-hydraulic performance in wavy fin-and-flat tube heat exchangers*, Applied Thermal Engineering, 30 (2010), 11-12, 1377-1386.

[12] Ay, H., Jang, J., Yeh, J-N.: *Local heat transfer measurements of plate finned-tube heat exchangers by infrared thermography*, International Journal of Heat and Mass Transfer, 45 (2002), 20, 4069-4078.

[13] Thole, K. A., Springer, M. E.: *Experimental design for flowfield studiesof louvered fins.* Experimental Thermal and Fluid Science, 18 (1998), 3, 258-269.

[14] Cebula, A., Taler, D.: *Determining thermal contact resistance of the fin-to-tube attachment plate in fin-and-tube heat exchanger,* 2nd International Conference on Engineering Optimization, Lisabon, Portugal, 2005.

[15] Liu, H., Kakac, S.: *Heat exchangers selection, rating and thermaldesign,* CRC Press, 2002.

[16] Malalesekera, W., Versteeg, H. K.: *An introduction to computational fluid dynamics, the finite volume method,* Prentice Hall, 1995.